Journal of Solid State Chemistry 295 (2021) 121916

Contents lists available at ScienceDirect

Journal of Solid State Chemistry

journal homepage: www.elsevier.com/locate/jssc

Novel luminescent calixarene-based lanthanide materials: From synthesis and characterization to the selective detection of Fe^{3+}

Ilária Martina Silva Lins [a], José Daniel da Silva Fonseca [a], Leonis Lourenço da Luz [a], Jarosław Chojnacki [b], Severino Alves Júnior [a], Bráulio Silva Barros [c,*], Joanna Kulesza [a,**]

[a] Universidade Federal de Pernambuco, Departamento de Química Fundamental, Av. Jornalista Anibal Fernandes, Cidade Universitária, 50740-560, Recife, PE, Brazil
[b] Department of Inorganic Chemistry, Chemical Faculty, Gdansk University of Technology, G. Narutowicza 11/12 Street, 80-233 Gdansk, Poland
[c] Universidade Federal de Pernambuco, Departamento de Engenharia Mecânica, Av. da Arquitetura, Cidade Universitária, 50740-550, Recife, PE, Brazil

ARTICLE INFO

Keywords:
Calix[4]arene
Coordination networks
Dinuclear complex
Luminescence
Sensors
Fe^{3+}

ABSTRACT

Calix[n]arene-based coordination networks are an emerging class of materials with intriguing properties resulted from the presence of the cavity-like structure of the macrocycle and metallic nodes. In this work, four novel luminescent materials based on calix[4]arene-carboxylate and lanthanides (Eu^{3+} and Tb^{3+}) were prepared by two synthetic approaches, solvothermal (CDA-Eu-ST) and slow diffusion (CDA-Eu-RT, CDA-Tb-RT, CTA-Tb-complex) methods. The coordination networks were characterized by PXRD, FTIR, SEM and solid-state photoluminescence, and the results indicated the formation of two different CDA-Eu-structures governed by the synthesis parameters. Single-crystal X-ray diffraction of CTA-Tb-complex revealed the formation of a new dinuclear complex of calix[4]arene-tetracarboxylate containing Na^{+} and Tb^{3+} coordinated within the lower rim of the molecule. Preliminary studies showed that CDA-Eu-RT was capable of selectively sensing Fe^{3+} ions in water via quenching the luminescence, demonstrating the possibility of using calix[4]arene-based platforms as efficient luminescent sensors.

1. Introduction

In the last two decades, coordination polymers and networks, including Metal-Organic Frameworks (MOFs), gained considerable attention of the scientific community. These materials are composed of an organic linker and an inorganic unit (ion or cluster) joined by coordination bonds [1,2]. Due to their structural versatility and tunable pore size, porous coordination polymers found potential for a wide range of application in drug adsorption and delivery [3,4], gas storage [5], volatile compounds adsorption and separation [6,7], chemical sensing [8], energy storage devices [9–12], and catalysis [13].

Materials based on lanthanides, such as LOFs (Lanthanide-Organic Frameworks), possess interesting photoluminescent features, like high quantum luminescence efficiency, long lifetimes, narrow bands, and large Stokes shift [14]. Combined with the intrinsic properties of MOFs, these materials are considered outstanding candidates as luminescent sensors for the detection of pollutants, like metal ions (Fe^{3+}, Al^{3+} [15], anions (CrO_4^{2-}, $Cr_2O_7^{2-}$) [16,17], explosives [18,19], and many others.

The detection of inorganic metal ions is important due to the increasing metal content in wastewater and soil, which cannot be easily biodegraded as organic contaminants. On the other hand, inorganic ions play a crucial role in living organisms. Iron is one of the most important elements of the human body. The Fe^{3+} ion influences important vital cell functions such as hemoglobin formation, allowing oxygen transport in blood, muscle and brain function, DNA synthesis, among others. However, both the lack and the excess of the normal iron limit can cause disorders to organisms. Iron deficiency can limit the delivery of oxygen to cells, resulting in fatigue and decreased immunity [20]. Thus, the selective detection of Fe^{3+} is a significant object of investigation. Numerous researchers have shown the potential applicability of LOFs for the detection of Fe^{3+} ions [17,19,21,22]. Nevertheless, most of these studies focus on organic system solvents, and investigation in aqueous solutions are rare. Thus, the development of efficient luminescent platforms for the selective detection for Fe^{3+} in water is still required. The main mechanism beyond the efficient luminescent process of sensing is associated with the host-guest interaction between coordination frameworks and

* Corresponding author. Universidade Federal de Pernambuco, Departamento de Engenharia Mecânica, Av. da Arquitetura, Cidade Universitária, 50740-550, Recife, PE, Brazil.
** Corresponding author. Universidade Federal de Pernambuco, Departamento de Química Fundamental, Av. Jornalista Anibal Fernandes, Cidade Universitária, 50740-560, Recife, PE, Brazil.
E-mail addresses: braulio.barros@ufpe.br (B.S. Barros), joanna.kulesza@ufpe.br (J. Kulesza).

https://doi.org/10.1016/j.jssc.2020.121916
Received 5 October 2020; Received in revised form 9 December 2020; Accepted 12 December 2020

guest molecules [23]. Interesting in this aspect are calix[n]arene-based luminescent materials.

Calix[n]arenes are phenolic based macrocycles consisting of n units of phenol linked by methylene groups [24]. The most stable are calixarenes with four phenolic units, called calix[4]arenes, which have been recently used for the construction of a variety of supramolecular materials, including metal-organic complexes [25–27], coordination networks, coordination polymers, and MOFs [6,28–31]. However, lanthanide-based calix[n]arene coordination networks are rare [32,33], and their potential application in sensing has not been reported so far.

Calixarene-lanthanide complexes have also been considered as interesting materials for investigation. Sandwich-like hexanuclear Tb-complex has shown single-molecule magnet behavior and photoluminescence [34]. Such bifunctional calixarene-lanthanide complexes can be found in the literature [35–37]. Ogden et al. have reported the preparation of transparent hybrid materials using calix[4]arene sensitized lanthanoid complexes incorporated into polymeric matrices [38].

In this work, four different calix[4]arene-based lanthanide materials (dinuclear complex and coordination networks) were prepared, and their luminescent properties have been investigated in the solid-state. Moreover, the Eu-based coordination network was tested for the sensing of different inorganic metal ions in water and showed the selectivity for Fe^{3+} ions based on luminescence quenching effects.

2. Experimental

2.1. Material and methods

Potassium carbonate (K_2CO_3), magnesium sulfate ($MgSO_4{\cdot}7H_2O$), sodium hydroxide (NaOH) were acquired from Dinâmica; methyl iodide (CH_3I), sodium hydride (NaH), ethyl bromoacetate ($BrCH_2COOC_2H_5$), *p-tert*-butylphenol, formaldehyde (37%) were purchased from Sigma-Aldrich. Europium (Eu_2O_3) and terbium (Tb_3O_4) oxides were purchased from Sigma-Aldrich and were used as received to prepare the corresponding lanthanide chlorides by treatment with concentrated hydrochloric acid (HCl). In the preparation of terbium chloride, hydrogen peroxide was also added to reduce Tb^{4+} to Tb^{3+}. Solvents; dimethylformamide (DMF), acetonitrile (ACN), acetone, dichloromethane (CH_2Cl_2), chloroform ($CHCl_3$), methanol (MeOH), *n*-hexane, toluene, ethanol (EtOH), ethyl acetate, hydrogen peroxide (H_2O_2), glacial acetic acid, diphenyl ether, and hydrochloric acid (HCl) were purchased from Dinâmica. Deuterated solvents $CDCl_3$ and DMSO for NMR analyses were purchased from Sigma Aldrich.

Single-crystal X-ray diffraction analysis was performed on an IPDS 2T dual-beam diffractometer (STOE & Cie GmbH, Darmstadt, Germany) at 120.0 (2) K with MoKα radiation of a microfocus X-ray source (GeniX 3D Mo High Flux, Xenocs, Sassenage, 50 kV, 1.0 mA, $\lambda = 0.71069$ Å). The investigated crystal was thermostated in the nitrogen stream at 120 K using CryoStream-800 device (Oxford CryoSystem, UK) during the entire experiment. Data collection and data reduction were controlled by X-Area 1.75 program [39]. Absorption correction was performed on the integrated reflections by a combination of frame scaling, reflection scaling, and a spherical absorption correction. The structures were solved by intrinsic phasing methods (SHELXT [40]) and refined anisotropically using the program packages SHELXL [41] and OLEX2 [42]. Positions of the C–H hydrogen atoms were calculated geometrically and taken into account with isotropic temperature factors. Water H-atoms were refined as riding on their parent atoms using a rotating group model. Visualization, and analysis of crystal structure were performed using the program *Mercury 4.0* [43].

Powder X-ray diffraction patterns were recorded on a Siemens diffractometer model D5000 using CuK_α ($\lambda = 1.5406$ Å) radiation with Ni filter, at voltage 30 kV and 10 mA. Experiments were conducted at 2θ values ranging from 5 to 50° with a step of 0.02°. The simulated PXRD pattern was obtained using the program *Mercury 2020.1*. Fourier transform infrared (ATR-FTIR) experiments were carried out on a Bruker Vertex 70/v spectrometer at the range of 4000–400 cm^{-1}. Morphological analyses and images were acquired on a Scanning Electron Microscopy (SEM), model Tescan Mira 3.^{1}H NMR spectra were acquired in an NMR spectrometer Agilent 400 MHz at 298 K in 5 mm NMR tube.

2.2. Synthesis

2.2.1. Preparation of p-tert-butylcalix[4]arene and carboxylate derivatives

p-tert-Butylcalix[4]arene was synthesized according to the synthetic approach reported by Gutche and Iqbal [44]. The derivative *p-tert*-butyl-25,26,27,28-tetrakis (carboxymethoxy)calix[4]arene (CTA) in *cone* conformation, was prepared according to the reported method [45] by hydrolysis of the corresponding calix-tetra-ester (CTE) [46]. The derivative *p-tert*-butyl-25,27-dicarboxy-26,28-dimethoxy calix[4]arene (CDA) was obtained following the literature procedure (with minor modification) in three steps involving the synthesis of i) calix-di-ether [47], ii) calix-di-ether-di-ester (in this case, toluene was used as the solvent instead of DMF) [48], iii) calix-di-ether-di-acid [49]. Spectral data of the compounds are placed in SI.

2.2.2. Preparation of CTA-Tb-complex

The sample CTA-Tb-complex was prepared according to our previous procedure [32] with some modifications: CTA (53 mg, 0.06 mmol) was dissolved in 6 mL of DMF, and the solution was transferred to a beaker containing an ACN solution (6 mL) of terbium chloride (0.06 mmol). The pH of the solution was adjusted to 1 with 1 M HCl. The mixture was left standing at room temperature without stirring. After 1 month, the crystals were isolated, collected by filtration, washed with DMF and dried at 60 °C for 2 h. For single-crystal X-ray diffraction measurements, crystals of CTA-Tb-complex were taken directly from the mother liquid solution without drying.

Selected bands on FTIR ν [cm^{-1}]: 3400 (OH); 2959–2866 (C–H); 2273 (C═N); 1786 (COOH); 1642 ν_{as} (COO^-) and 1485 ν_s (COO^-).

2.2.3. Preparation of CDA-Ln coordination networks (Ln = Eu, Tb)

The procedure for the preparation of CDA-Ln coordination networks was adapted from the literature [32,33]: 1 mmol of $LnCl_3.6H_2O$ (Ln = Eu or Tb), was dissolved in DMF while 3 mmols of the ligand (CDA) were dissolved in a mixture of DMF and ACN. Both solutions were mixed, and the resulting solution was either left to stand for 1 month at room temperature (slow evaporation method) or transferred to the reactor and heated in an oven at 90 °C for 4 days (solvothermal method). At the end of each synthesis, the powder was washed with DMF and ACN, filtered and allowed to dry in air. The products were labelled as CDA-Eu-RT, CDA-Tb-RT, and CDA-Eu-ST, for samples prepared by slow evaporation and solvothermal method, respectively.

CDA-Eu-RT Selected bands on FTIR ν [cm^{-1}]: 2959–2866 (C–H); 1747 (COOH); 1644 ν_{as} (COO^-) and 1478 ν_s (COO^-). **CDA-Tb-RT** Selected bands on FTIR ν [cm^{-1}]: 2959–2866 (C–H); 1747 (COOH); 1644 ν_{as} (COO^-) and 1478 ν_s (COO^-). **CDA-Eu-ST** Selected bands on FTIR ν [cm^{-1}]: 2959–2866 (C–H); 1664 (C═O, DMF); 1573 ν_{as} (COO^-); 1428 ν_s (COO^-) and 1478 ν_s (COO^-).

2.3. Luminescence

2.3.1. General

The photoluminescence properties were investigated at room temperature using a spectrofluorometer Horiba-Jobin Yvon Fluorolog-3 with a continuous 450 W xenon lamp and 150 W xenon flash tube for excitation, double-grating monochromator in the excitation and UV-VIS (ultraviolet–visible) emission position, single-grating monochromator in the NIR (near-infrared) emission position, R928P and H10330A-75 Hamamatsu photomultipliers respectively to UV-VIS range emissions. All emission spectra were corrected for the wavelength-dependent response of the detection system. A silicon photodiode reference detector was used to monitor and compensate the variation in the xenon lamp

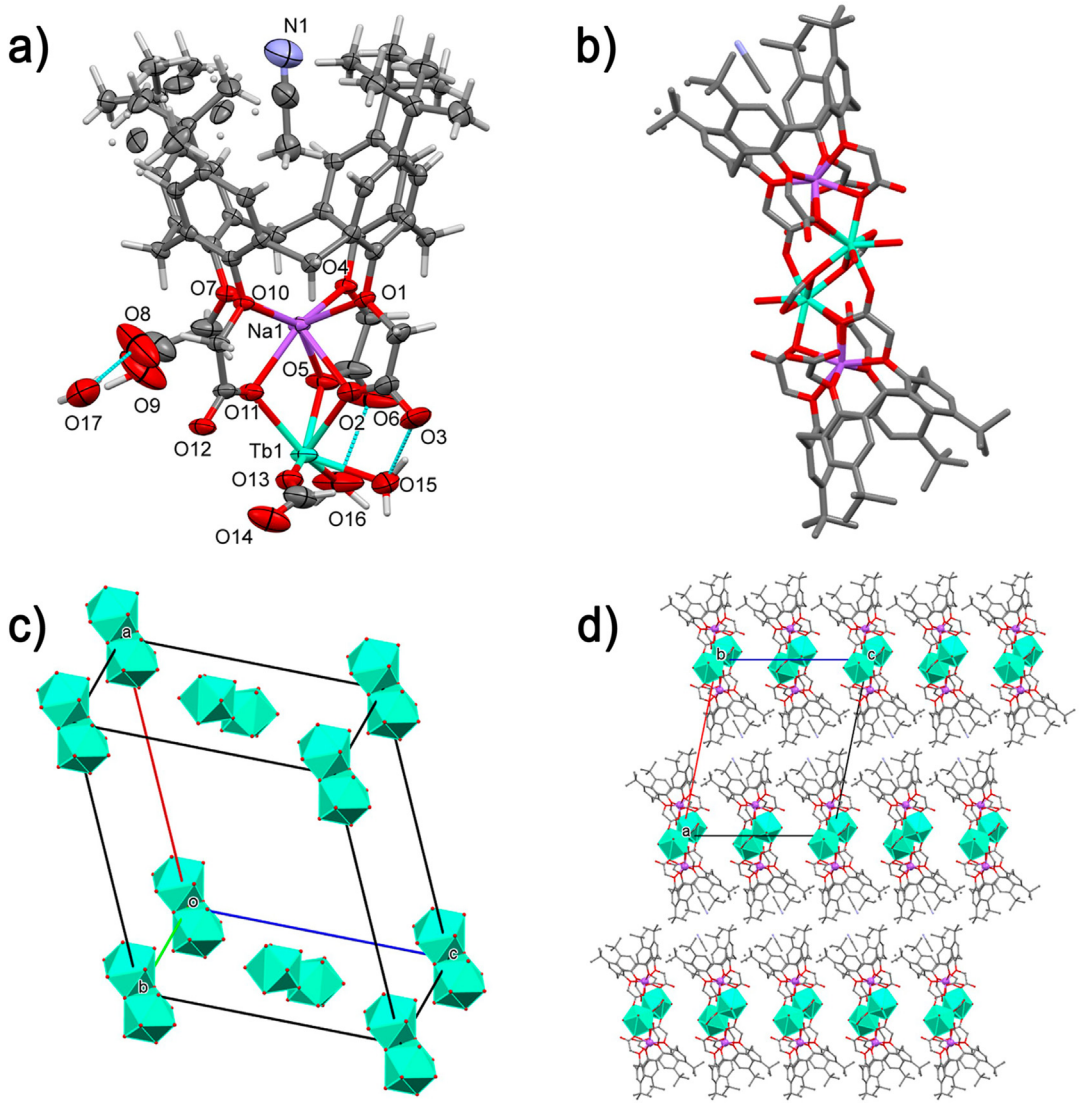

Fig. 1. a) Atom labeling in the asymmetric unit, b) molecular view of the dimer, c) partial view of the unit cell showing only the coordination polyhedra of Tb^{3+} ions, and d) view along the y-axis of the crystal packing for CTA-Tb-complex. Displacement ellipsoids drawn at 50% probability level, hydrogen bonding drawn as hashed lines, hanging contacts deleted.

output, using typical correction spectra provided by the manufacturer. Measurements of luminescence lifetimes were performed on the same spectroscopic apparatus but with a 150 W xenon flash lamp.

The luminescence lifetime (τ) was obtained by fitting radiative decay curves, using equation (1):

$$I(t) = \sum_i B_i e^{(-t/\tau_i)} \quad (1)$$

where I is the emission intensity, B_i is a pre-exponential factor, t is time, and τ_i is the lifetime.

The emission quantum efficiency (η) was calculated according to Equation (2), where A_{rad} is the radiative decay rate obtained by summing over the radiative rates $A_{0,J}$ for each $^5D_0 \rightarrow {}^7F_J$ (J = 0–4) transitions. The total radiative decay rate (A_{total}) is given by the relation $A_{total} = \tau^{-1}$, where τ is the lifetime for the emission-decay curve associated with the $^5D_0 \rightarrow {}^7F_2$ transition. Finally, the non-radiative decay rate (A_{nrad}) is given by the difference $A_{nrad} = A_{total} - A_{rad}$ [50].

$$\eta = \frac{A_{rad}}{A_{rad} + A_{nrad}} \text{ x } 100\% \quad (2)$$

2.3.2. Metal ion sensing

The experimental approach used for the sensing of metal ions were adapted from the literature [19]. The assays were divided into three stages: i) evaluation of the luminescence response of CDA-Eu-RT in the presence of different solvents; ii) study of the luminescence response of CDA-Eu-RT towards different metal ions (Li^+, Al^{3+}, Pb^{2+}, Cu^{2+}, Zn^{2+}, Cd^{2+}, Fe^{3+}); iii) studies in different concentrations of the metal with the best response.

To investigate the luminescence response of CDA-Eu-RT in different solvents, 5 mg of the sample CDA-Eu-RT were dispersed in 10 mL of distilled water or DMF. The solutions were prepared using an ultrasonic probe SONICS Vibra-cell model VC 505, employing 50% of the total power (500 W) for 10 min in a sequence of pulses 4 s on, and 6 s off. After ultrasound treatment, resulting suspensions were left standing for one day for sedimentation of large particles (stock solution). Then a fine colloidal suspension was separated from residue of large particles, and the luminescence analyses were performed.

For tests with different metals, 1 mL of the CDA-Eu-RT stock solution in distilled water and 1 mL of the 0.1 M nitrate solution containing the studied cation were mixed in a quartz cuvette, and subsequently, the emission spectrum was recorded. Based on the results for each cation,

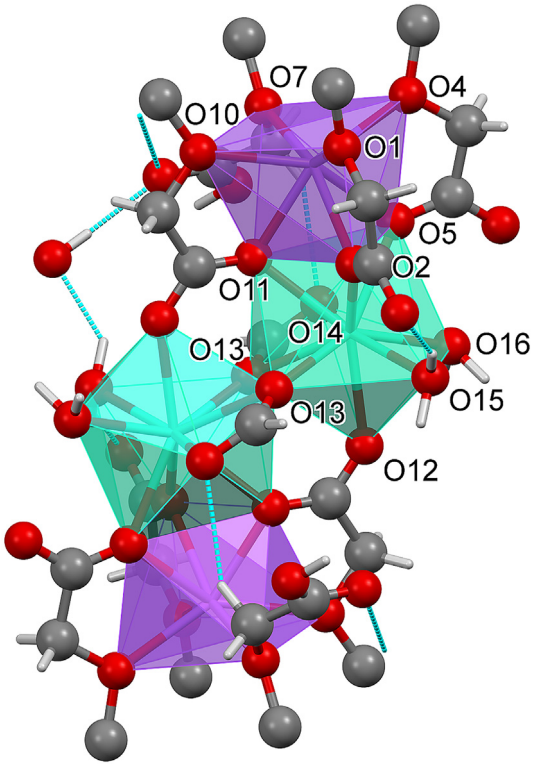

Fig. 2. View of terbium and sodium coordination polyhedra in the center of the molecular dimer. Calixarene residues were truncated up to phenyl C–O carbon atoms for clarity. Only donor O-atoms are labelled in one part of the dimer. Atoms, in the other part, are related by inversion. Hydrogen bonds are drawn as hashed lines. Two terbium polyhedra have a common edge (O13–O13 [2-*x*,1-*y*,1-*z*]), while sodium and terbium polyhedra have one common trigonal face (O2–O5–O11).

Fe^{3+} ion was chosen to proceed with studies on different concentrations of the metal (1×10^{-3} to 1 mmol L^{-1}). In each test, 0.5 mL of Fe^{3+} solution was transferred to a quartz cuvette, and then 0.5 mL of the aqueous suspension of the CDA-Eu-RT was added, the sample was homogenized, and after approximately 2 min, the emission spectra ($\lambda_{ex} = 287$ nm) were recorded.

3. Results and discussion

3.1. Structure description

The synthesis of CTA-Tb-complex led to the formation of single crystals suitable for X-ray analysis, whereas for other materials, all trials failed in producing adequate crystals.

CTA-Tb-complex crystallizes in the monoclinic system, space group $P2_1/c$ (no. 14), Z = 2. The asymmetric unit contains half of the molecule, and due to the presence of the inversion center between terbium atoms, the whole molecule is a dinuclear complex, shown in Fig. 1. Experimental details for CTA-Tb-complex are summarized in Table S1.

Interestingly, the temperature of the reaction was a key factor for obtaining a sandwich-like complex. In our previous work, the same reaction conducted at 90 °C for 24 h led to the formation of a mononuclear complex [32].

In CTA-Tb-complex, calix[4]arene is in common *cone* conformation with dihedral angles between opposite phenyl rings equal to 43.05 (15)° and 51.51 (15)° (C1–C6 to C27–C32 and C14–C19 to C40–C45, respectively). Each of the calixarene residues is triply deprotonated, with a sodium cation solvated within the lower rim of the calix. We assume that Na^+ may originate from the synthesis of the calixarene derivative, where NaOH was used for hydrolysis.

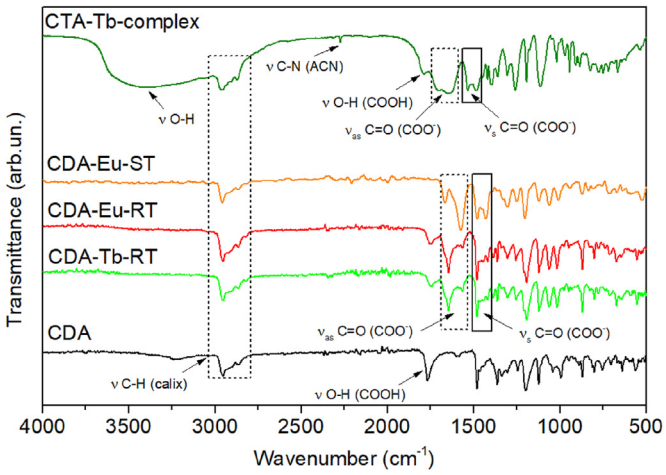

Fig. 3. FTIR spectra of the synthesized CDA-Ln samples (Ln = Eu, Tb), CTA-Tb-complex, and the ligand CDA.

The cation is surrounded by etheric and carboxylate oxygen atoms. The coordination number of Na^+ is seven since one carboxyl group (the protonated one) is directed outside, and only the etheric oxygen atom takes part in the coordination of sodium. Evidence of protonation is found in the FTIR spectrum and relatively long C38–O9 bond of the hydroxyl group, 1.344 (7) Å, while other carboxylic C–O bonds are in the range 1.21–1.27 Å. The other oxygen atoms of the three carboxylic anions are bridging to the terbium cation. The coordination number of Tb^{3+} is nine including also: two water molecules O15, O16, three O-atoms from two bridging formate anions H–COO^- and one oxygen atom O17 from another calixarene molecule related by inversion (see Fig. 1, only six bonds are present within the asymmetric unit).

The HCOO- anions originated from the hydrolysis of DMF used in the synthesis according to equations (3) and (4)).

$$HCON(CH_3)_2 + H_2O \; HCOOH + (CH_3)_2NH \quad (3)$$

As the products of hydrolysis are weakly acidic and weakly basic, respectively, they ionize originating formate anions and dimethylamine cations:

$$HCOOH + (CH_3)_2NH \rightleftarrows HCOO^- + (CH_3)_2NH_2^+ \quad (4)$$

Additionally, inside each calixarene cavity, one acetonitrile molecule is included, with a polar cyano group directed outside the calix, and one water molecule (O18) is linked to the second coordination sphere of Tb^{3+} and O8 atom from the protonated carboxylic group. Thus, formally one can describe the molecule as $[\{(calix^{3-})\,(HCOO^-)\,(Na^+)\,(Tb^{3+}(H_2O)_2)\}_2,\ 2\ CH_3CN,\ 2H_2O]$. The discrete dimeric coordination compounds (Fig. 2) are linked in the crystalline phase by hydrogen bonding (see Table S2 for details) provided by the bridging O17 water molecule. Terbium cations are separated by the distance of 4.02371 (4) Å in the dimer and are bridged by two carboxylate anions and two formyl anions (labelled O11, O12, and O13).

3.2. Sample characterization

3.2.1. FTIR

The FTIR spectra of the obtained CDA-Ln samples, CTA-Tb-complex, and the ligand CDA are shown in Fig. 3.

The strong band at 1764 cm^{-1}, observed in the ligand spectrum, corresponds to the stretching vibration ν (C═O) of the COOH groups. New bands in the spectra of CDA-Eu-RT and CDA-Tb-RT at 1644 and 1478 cm^{-1}, corresponding to the stretching asymmetric and symmetric vibrations of deprotonated COO^- carboxylate groups, respectively, indicate the formation of coordination networks. The spectra of CDA-Eu-

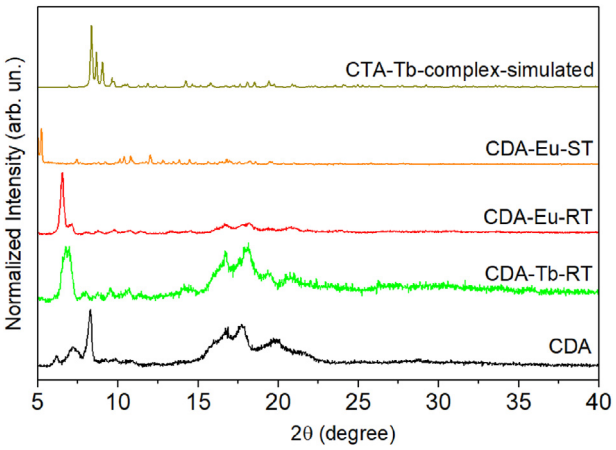

Fig. 4. PXRD patterns of the synthesized CDA-Ln samples (Ln = Eu, Tb) and of the ligand CDA, in comparison with the simulated from single-crystal data XRD pattern of CTA-Tb-complex.

RT and CDA-Tb-RT are comparable, suggesting the formation of structurally similar materials. On the other hand, the FTIR spectrum of CDA-Eu-ST is quite different from those of other hybrid materials; thus, one can assume that this sample present a distinct structure. The presence of intense bands at 1573 and 1428, 1478 cm^{-1}, suggest the formation of COO-Eu coordination bonds. The residual band at 1664 cm^{-1} may be ascribed to the stretching C═O vibration of the DMF molecule present in the structure. Although further evidence should be furnished, the prepared CDA-Ln samples could not be dissolved in any organic solvent that may indicate the formation of a polymer structure.

In the FTIR spectrum of the CTA-Tb-complex, some bands related to the stretching asymmetric and symmetric vibrations of deprotonated COO^- carboxylate groups are visible, in addition to the residual band at 1786 cm^{-1} attributed to the stretching vibration ν (C═O) of the protonated COOH groups. Moreover, bands corresponding to the stretching vibrations of O–H and C≡N groups at 3400 and 2273 cm^{-1}, respectively, confirm the presence of water and acetonitrile in the complex, in agreement with the described crystal structure. Bands in the region of 3000 cm^{-1} related to the stretching vibrations of C–H groups are further evidence of calixarene molecules in all samples.

3.2.2. PXRD

The powder X-ray diffraction patterns of the samples CDA-Eu-RT, CDA-Tb-RT, and CDA-Eu-ST, were compared with the PXRD pattern of the ligand CDA and with the simulated pattern from the single-crystal structure of CTA-Tb-complex (Fig. 4). The powder diffraction patterns of CDA-Eu-RT, CDA-Tb-RT, and CDA-Eu-ST present diffraction patterns different from the expected for CTA-Tb-complex, indicating the formation of new materials. These peaks appear in lower angles than for a CDA-Tb-complex, suggesting bigger unit cells, which is rather typical for coordination networks containing calixarenes. However, diffraction peaks between 15 and 25° observed in the case of CDA-Tb-RT match with the

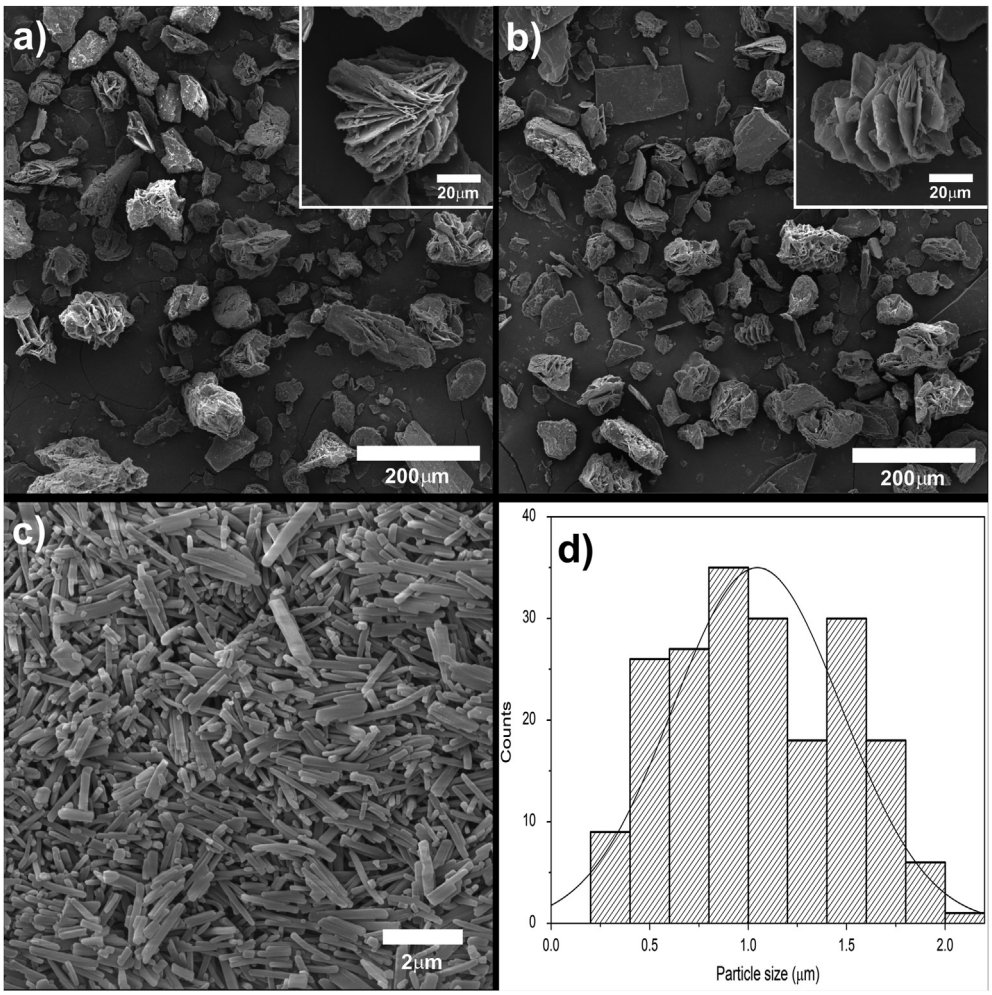

Fig. 5. SEM images of the CDA-Ln samples prepared at room temperature a) CDA-Eu-RT, b) CDA-Tb-RT, and by the solvothermal method, c) CDA-Eu-ST. d) Particle size (length) histogram for CDA-Eu-ST.

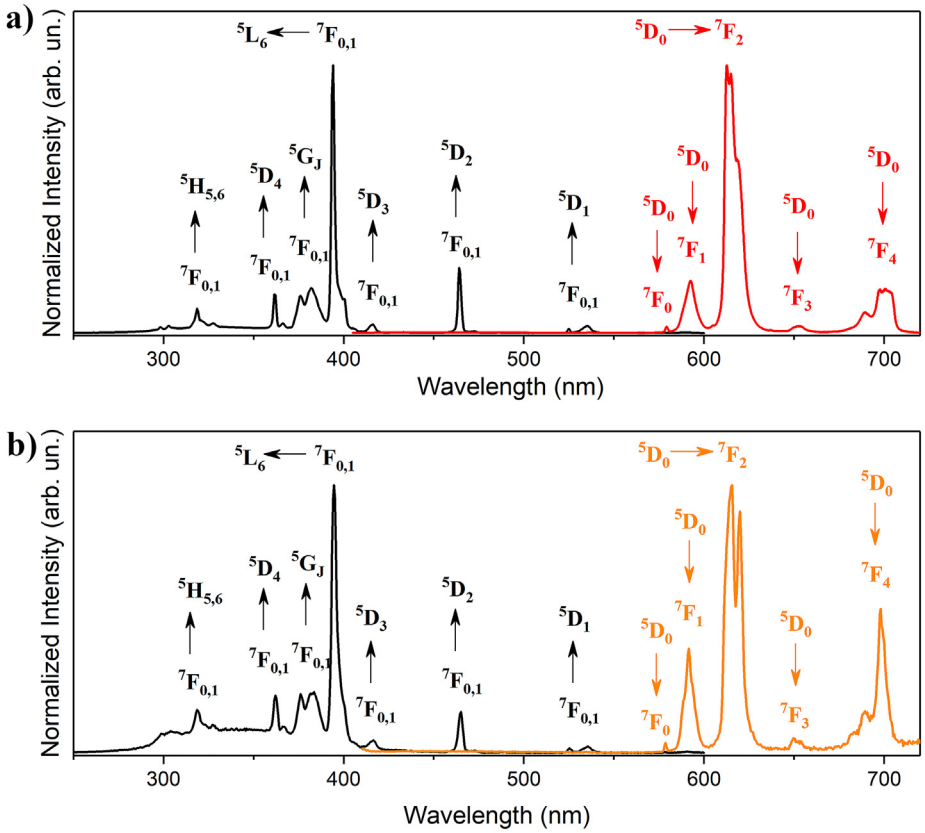

Fig. 6. Excitation (λ_{em} = 615 nm) and emission (λ_{ex} = 395 nm) spectra of a) CDA-Eu-RT and b) CDA-Eu-ST obtained in the solid-state at room temperature.

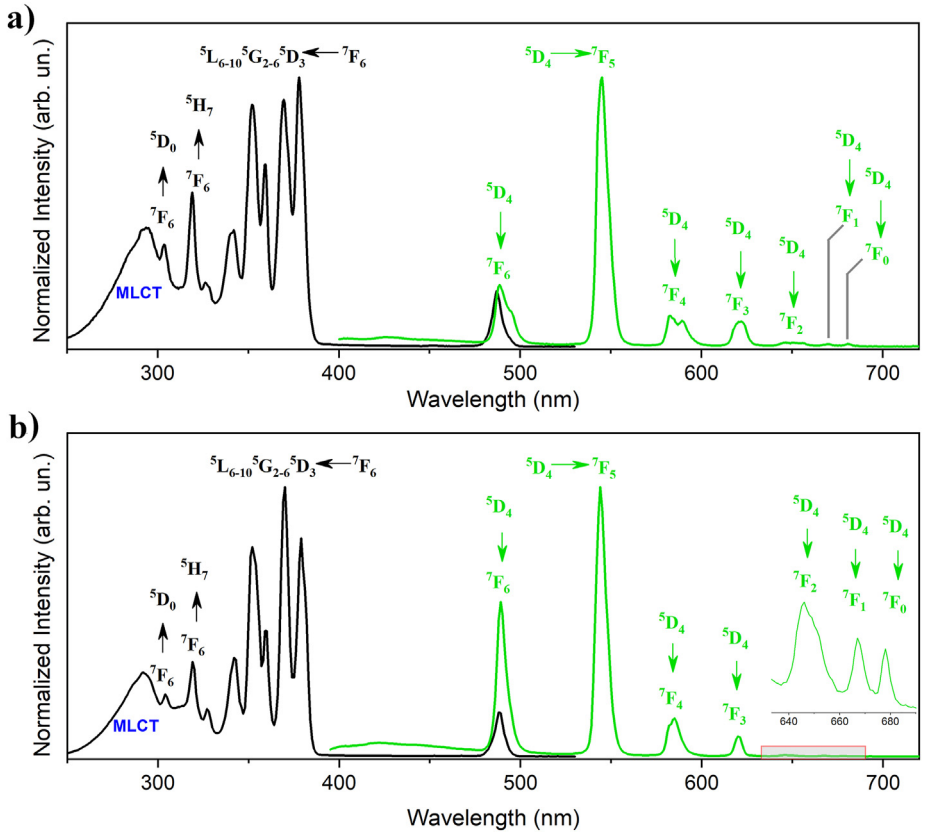

Fig. 7. Excitation (black line) and emission (λ_{ex} = 378 nm) spectra of a) CDA-Tb-RT and b) CTA-Tb-complex obtained in the solid-state at room temperature.

peaks corresponding to the ligand, suggesting the presence of the unreacted CDA ligand in the sample. Although it was impossible to identify the obtained phases, it can be seen that the X-ray diffraction pattern of CDA-Eu-ST is quite different from that obtained for the sample CDA-Eu-RT showing that the use of different temperatures in both syntheses led to two structurally different networks, in agreement with the FTIR results.

3.2.3. SEM

The micrographs of the CDA-Ln samples and the histogram of particle length for CDA-Eu-ST are shown in Fig. 5. The particles of materials synthesized via different methodologies have a different shape, size, and dispersion. The samples obtained at room temperature (CDA-Eu-RT and CDA-Tb-RT) (Fig. 5a and b) present similar morphology with agglomerated particles of lamellar structure, without defined contours and high size dispersion (>20 μm). The sample obtained via the solvothermal method, CDA-Eu-ST (Fig. 5c), presents homogeneous morphology in the form of rods with narrow size distribution and the average length of 1 μm (Fig. 5d).

3.3. Photoluminescent properties

The photoluminescence behavior of all materials was investigated in the solid-state at room temperature. The excitation spectra (black lines of Fig. 6) of CDA-Eu-RT and CDA-Eu-ST obtained by monitoring the emission at 615 nm ($^5D_0 \rightarrow {}^7F_2$) are similar and presents only the bands assigned to the characteristic *f-f* Eu^{3+} transitions, indicating that the CDA ligand does not act as an efficient antenna for Eu^{3+} ion luminescence sensitization.

The emission spectra of CDA-Eu-RT and CDA-Eu-ST were obtained under excitation at 395 nm (red line, Fig. 6a, and b, respectively). The spectral profile shows peaks corresponding to the $^5D_0 \rightarrow {}^7F_J$ transitions (J = 0, 1, 2, 3, 4) of the Eu^{3+} ion, with the most intense band at 615 nm of $^5D_0 \rightarrow {}^7F_2$ transition corresponding to 70% and 52% of the total area of the spectrum, for CDA-Eu-RT and CDA-Eu-ST, respectively, which confers red photoluminescence to the materials. The strong intensity of the $^5D_0 \rightarrow {}^7F_2$ (electric dipole) transition relative to $^5D_0 \rightarrow {}^7F_1$ (magnetic dipole) transition I ($^5D_0 \rightarrow {}^7F_2$)/I ($^5D_0 \rightarrow {}^7F_1$) equal to 5.22 and 2.63 for CDA-Eu-RT and CDA-Eu-ST, respectively) and the presence of the peak attributed to the strongly forbidden electric dipole $^5D_0 \rightarrow {}^7F_0$ transition in both spectra indicates that the Eu^{3+} ions are embedded in a low symmetry environment without inversion center, typically C_n, C_{nv} or C_s. Moreover, the presence of a single, symmetrical peak of the $^5D_0 \rightarrow {}^7F_0$ transition, together with a single exponential profile of the decay emission intensity (Figure S1), indicates that in each material, only one type of coordination environment around Eu^{3+} is present. On the other hand, the analysis of the spectral profile (split and relative intensity) of each Eu^{3+} emission peak suggest a distinct symmetry environment around Eu^{3+} ions in each material [51]. In addition, the high asymmetry ratio of the CDA-Eu-RT, equal to R = (I ($^5D_0 \rightarrow {}^7F_2$)/I ($^5D_0 \rightarrow {}^7F_1$)) = 5.13 is similar to our previously published results for a calixarene-tetracarboxylate Eu-coordination polymer (R = 5.22) [32] but much greater than for a typical calixarene-Eu^{3+} inclusion complex (R = 2.73) [51].

It was also found that CDA-Eu-RT presented a quantum efficiency of 38%, which is much higher than for our calixarene-tetracarboxylate Eu-coordination polymer (20.3%) [32] and other calixarene-based systems [52]. In the case of CDA-Eu-ST, the quantum efficiency was lower and equal to 21%.

The monoexponential fit of luminescence decay curves for CDA-Eu-RT (Figure S1a) and CDA-Eu-ST (Figure S1b) gave lifetime values of 0.84 and 0.76 ms, respectively. These values are higher than for our previously reported Eu-hybrid material (τ = 0.46 ms) [32].

The excitation spectrum of the CDA-Tb-RT and CTA-Tb-complex (Fig. 7), obtained by monitoring the emission at 547 and 545 nm, respectively, exhibits a wide band in the region between 250 and 330 nm

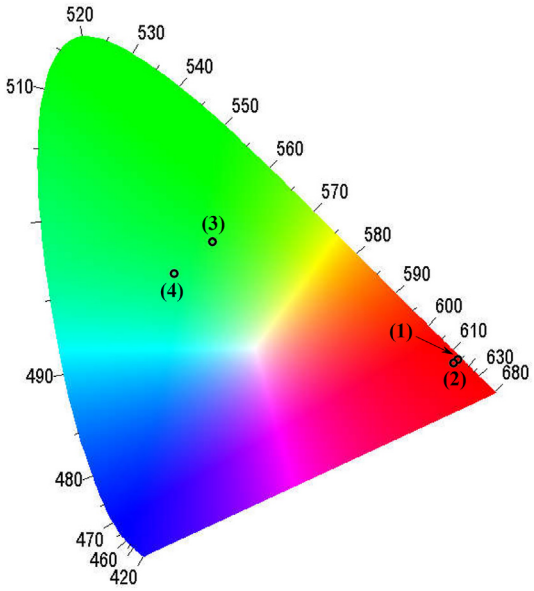

Fig. 8. CIE chromaticity diagram indicating the color coordinates points of the CDA-Eu-RT (1), CDA-Eu-ST (2), CDA-Tb-RT (3), and CTA-Tb-complex (4).

that can be attributed to the metal-ligand charge transfer (MLCT). The assignment to intraconfigurational 4f-5d transition was ruled out due to their typical energy occurrence [53]. However, additional experiments should be performed to avoid misinterpretations. In the region between 340 and 500 nm, bands related to the intraconfigurational *f-f* transitions of the Tb^{3+} ion are found.

Upon excitation, at 378 nm both CDA-Tb-TA and CTA-Tb-complex materials show the emission spectra composed by narrow emission bands assigned to the $^5D_4 \rightarrow {}^7F_J$ transitions (J = 0, 1, 2, 3, 4, 5, 6) of the Tb^{3+} ion, in which the $^5D_4 \rightarrow {}^7F_5$ transition is the most intense and main responsible by the green photoluminescence of the materials (Fig. 7). The luminescence decay curves of the CDA-Tb-TA and CTA-Tb-complex materials after excitation at 378 nm exhibits a monoexponential profile in

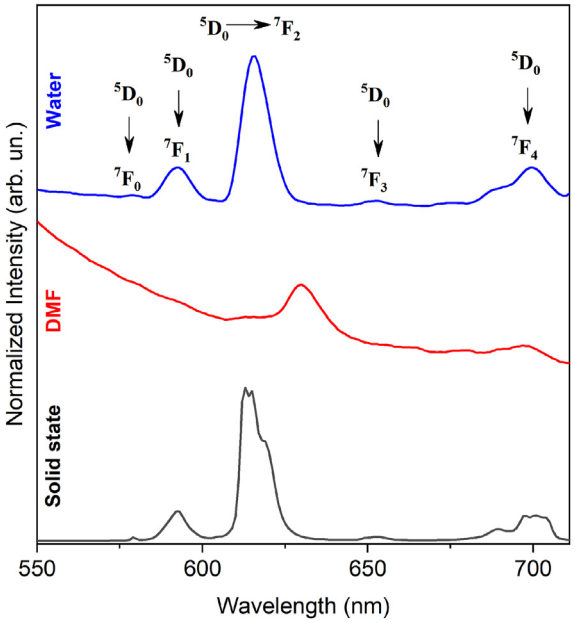

Fig. 9. Emission spectra of CDA-Eu-RT in the solid-state (λ_{ex} = 395 nm), dispersed in DMF (λ_{ex} = 395 nm), and water (λ_{ex} = 287 nm).

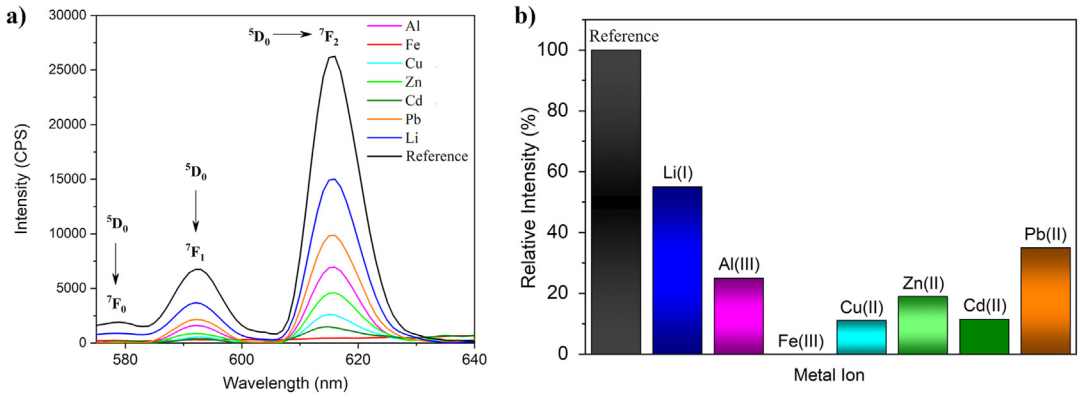

Fig. 10. (a) Emission spectra of CDA-Eu-RT (in water) in the presence of different metal ions. (b) Emission intensity bar diagram related to the transition $^5D_0 \rightarrow {}^7F_2$ (~616 nm) of the Eu^{3+} ion in the presence of different metal ions.

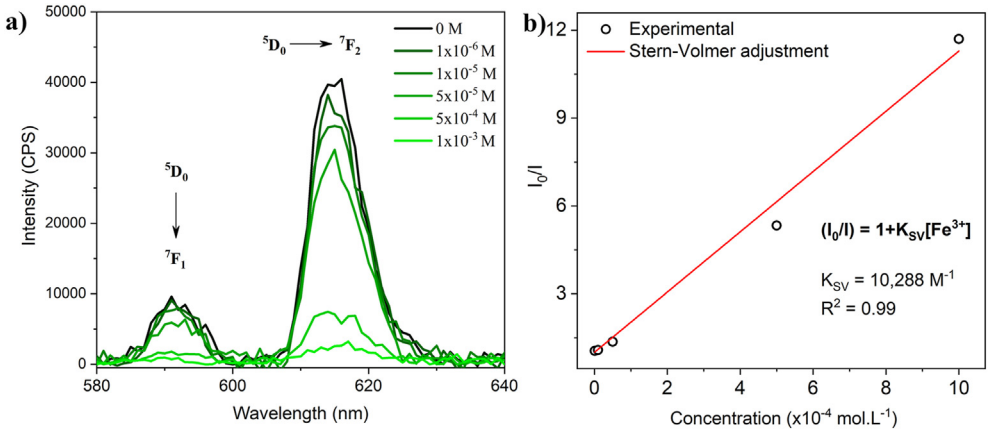

Fig. 11. (a) Emission spectrum of CDA-Eu-RT suspensions at different concentrations of Fe^{3+} ions. (b) plot I/I_0 vs. [C] in the detection of Fe^{3+} ions at different analyte concentrations (circles) and Stern−Volmer regression (red line).

which the exponential decay fit gave lifetimes of 0.84 and 0.76 ms, respectively (Figure S2). The color coordinate, dominant wavelength, and color purity were determined from the emission spectrum of each material, using the Commission International del'Eclairage- (CIE-) 1931 Standard Source color coordinate [illuminant C = (0.3101, 0.3162)] as a reference [54,55]. Fig. 8 shows the photoluminescence color coordinates (x, y) exhibited by the CDA-Eu-RT (0.674, 0.317), CDA-Eu-ST (0.666, 0.310), CDA-Tb-TA (0.282, 0.504), and CTA-Tb-complex (0.221, 0.453). The respective color purities are 96.8% (λ = 616 nm), 87.8% (λ = 619 nm), 19.5% (λ = 542 nm) and 9.3% (λ = 511 nm). To develop a colorimetric-based detection system, a LED photodetector can provide a compact analytical instrument with smaller amounts of sample volume and faster response times. For this, the analytical signal (emission of the sensing) needs to be the most color purity as possible [56]. Thus, only Eu-based compounds have a high color purity in which the CDA-Eu-RT is the most remarkable.

3.4. Luminescent sensing of metal ions

Based on the emitted color purity, the sample CDA-Eu-RT was chosen for preliminary tests for metal ions sensing in a liquid phase. Firstly, the stability of CDA-Eu-RT dispersed into nonprotic (DMF), and protic (water) solvents was investigated. The DMF possibly led to the collapse of the structure during the ultrasound treatment, confirmed by the drastic change in the spectral emission profile (Fig. 9). On the other hand, in the aqueous system, the emission spectral profile was maintained after ultrasound treatment (Fig. 9), suggesting greater stability of CDA-Eu-RT in an aqueous medium.

The sensing tests in the presence of the metal ions Li^+, Al^{3+}, Pb^{2+}, Cu^{2+}, Zn^{2+}, Cd^{2+}, Fe^{3+} (Fig. 10) show a significant decrease in the luminescence intensity of the Eu^{3+} ions present in CDA-Eu-RT. Analysing the integrated intensities related to the $^5D_0 \rightarrow {}^7F_2$ transition (616 nm), greater sensitivity is noticed for the Fe^{3+} ions, leading to the total suppression of the luminescence of Eu^{3+}.

Since the luminescence of CDA-Eu-TA showed greater sensitivity for Fe^{3+} ions compared to other ions, experiments in an aqueous medium containing different concentrations of Fe^{3+} ions (from 1×10^{-6} to 1×10^{-3} mol L^{-1}) were performed, and the emission spectra are shown in Fig. 11a. As can be seen, the luminescence intensity decreases with the increase in the analyte concentration (Fe^{3+}).

Using the areas (integrated intensity) of the transition $^5D_0 \rightarrow {}^7F_2$ for each concentration, the graph of the I_0/I ratio vs. [Fe^{3+}] was plotted (Fig. 11b), where I_0 corresponds to the initial intensity without the presence of Fe^{3+} ions (reference), I corresponds to the intensity in each concentration of Fe^{3+} and [Fe^{3+}] represents the concentration of the Fe^{3+} ions. To further quantitatively evaluate the quenching effect of Fe^{3+} ions, the Stern−Volmer equation ($I_0/I = 1 + K_{SV}$ [Fe^{3+}]) was used to calculate the quenching constants (K_{SV}). The emission ratio (I_0/I) exhibits a good linear correlation at the considered concentration range (R = 0.99). According to the Stern-Volmer equation, K_{SV} for CDA-Eu-RT is found to be 1.0288×10^4 M^{-1} (Fig. 11b). This quenching constant (K_{SV}) is comparable to those of the most reported MOF sensors ($1 \times 10^4 - 1 \times 10^5$ mM^{-1}), for this concentration range [57,58]. The above results clearly indicate a high sensitivity of the CDA-Eu-RT for Fe^{3+} ions in a water environment.

4. Conclusions

In summary, four novel luminescent calix [4]arene-based hybrid materials were prepared via solvothermal (CDA-Eu-ST) and slow diffusion (CDA-Eu-RT, CDA-Tb-RT, CTA-Tb-complex) methods. Different synthesis methods led to two structurally and morphologically different Eu-coordination networks, as suggested by PXRD, FTIR, SEM, and luminescent characterizations. CTA-Tb-complex is the first luminescent dinuclear complex based on calix [4]arene-tetracarboxylate, and Tb^{3+} reported so far. The preliminary luminescent sensing studies indicated that CDA-Eu-RT is a promising platform for the detection of Fe^{3+} in a water environment. This is the first example of the research devoted to the luminescent ion sensing by calix [n]arene-based coordination network. Further studies will involve a deeper investigation of the luminescent sensing of the system, including the turn-off luminescence mechanism, as well as other calix [n]arene-based platforms.

CRediT authorship contribution statement

Ilária Martina Silva Lins: Methodology, Investigation. **José Daniel da Silva Fonseca:** Methodology, Investigation. **Leonis Lourenço da Luz:** Investigation, Visualization, Writing - original draft. **Jarosław Chojnacki:** Investigation, Formal analysis, Writing - original draft. **Severino Alves Júnior:** Writing - review & editing, Resources. **Bráulio Silva Barros:** Formal analysis, Resources, Writing - original draft, Visualization, Writing - review & editing. **Joanna Kulesza:** Supervision, Conceptualization, Resources, Writing - original draft.

Declaration of competing interest

The authors declare that they have no known competing financial interests or personal relationships that could have appeared to influence the work reported in this paper.

Acknowledgments

The authors thank Universidade Federal de Pernambuco and Gdansk University of Technology. I. M. S. L. thanks the Brazilian Ministry of Education (MEC) for a scholarship granted from Tutorial Education Program. J. D. S. F. thank FACEPE and CAPES for a scholarship granted. L. L. L. thank the Chemistry Graduate Program at UFPE, FACEPE and PNPD-CAPES fellowships. This work was financially supported by CNPq and FACEPE (Grants no. 403747/2016–3, APQ-0818-1.06/15, APQ-0675-1.06/14). This study was financed in part by the Coordenação de Aperfeiçoamento de Pessoal de Nível Superior – Brasil (Capes) – Finance Code 001. We also acknowledge CEMENE and Central Analítica-DQF-UFPE for the support with the characterizations.

Appendix A. Supplementary data

Supplementary data related to this article can be found at https://doi.org/10.1016/j.jssc.2020.121916.

References

[1] H. Furukawa, K.E. Cordova, M. O'Keeffe, O.M. Yaghi, The chemistry and applications of metal-organic frameworks, Science 80 (2013) 341, https://doi.org/10.1126/science.1230444.
[2] B.S. Barros, O.J. deLimaNeto, A.C. deOliveiraFrós, J. Kulesza, Metal-organic framework nanocrystals, Chemistry 3 (2018) 7459–7471, https://doi.org/10.1002/slct.201801423.
[3] M. Al Haydar, H.R. Abid, B. Sunderland, S. Wang, Multimetal organic frameworks as drug carriers: aceclofenac as a drug candidate, Drug Des. Dev. Ther. 13 (2019) 23–35, https://doi.org/10.2147/DDDT.S182983.
[4] O.J. de Lima Neto, A.C. de O. Frós, B. Barros, A.F. de Farias Monteiro, J.E. Kulesza, Rapid and efficient electrochemical synthesis of a zinc-based nano-MOF for Ibuprofen adsorption, New J. Chem. 5 (2019) 5518–5524, https://doi.org/10.1039/c8nj06420b.
[5] J.R. Li, R.J. Kuppler, H.C. Zhou, Selective gas adsorption and separation in metal-organic frameworks, Chem. Soc. Rev. 38 (2009) 1477–1504, https://doi.org/10.1039/b802426j.
[6] A.C. de Oliveira Frós, M.A. de Oliveira, A.A. Macêdo Soares, F. Hallwass, J. Chojnacki, B.S. Barros, S.A. Júnior, J. Kulesza, Selective adsorption of BTEX on calixarene-based molecular coordination network determined by 13 C NMR spectroscopy, Inorg. Chim. Acta. 492 (2019) 161–166, https://doi.org/10.1016/j.ica.2019.04.031.
[7] L.F. Pereira, A.C. de Oliveira Frós, M.K. Manosso Amorim, F. Hallwass, L.C. Almeida, B.S. Barros, J. Kulesza, Ultrasound irradiation effect on morphological and adsorptive properties of a nanoscale 3D Zn-coordination polymer and derived oxide, Ultrason. Sonochem. 69 (2020) 105275, https://doi.org/10.1016/j.ultsonch.2020.105275.
[8] L.E. Kreno, K. Leong, O.K. Farha, M. Allendorf, R.P. Van Duyne, J.T. Hupp, Metal-organic framework materials as chemical sensors, Chem. Rev. 112 (2012) 1105–1125, https://doi.org/10.1021/cr200324t.
[9] K. Wang, R. Bi, M. Huang, B. Lv, H. Wang, C. Li, H. Wu, Q. Zhang, Porous cobalt metal-organic frameworks as active elements in battery-supercapacitor hybrid devices, Inorg. Chem. 59 (2020) 6808–6814, https://doi.org/10.1021/acs.inorgchem.0c00060.
[10] K. Wang, Q. Li, Z. Ren, C. Li, Y. Chu, Z. Wang, M. Zhang, H. Wu, Q. Zhang, 2D metal–organic frameworks (MOFs) for high-performance BatCap hybrid devices, Small 16 (2020) 1–6, https://doi.org/10.1002/smll.202001987.
[11] K. Wang, B. Lv, Z. Wang, H. Wu, J. Xu, Q. Zhang, Two-fold interpenetrated Mn-based metal-organic frameworks (MOFs) as battery-type electrode materials for charge storage, Dalton Trans. 49 (2020) 411–417, https://doi.org/10.1039/c9dt04101j.
[12] K.-B. Wang, Q. Xun, Q. Zhang, Recent progress in metal-organic frameworks as active materials for supercapacitors, Energy 2 (2020) 100025, https://doi.org/10.1016/j.enchem.2019.100025.
[13] J. Lee, O.K. Farha, J. Roberts, K.A. Scheidt, S.T. Nguyen, J.T. Hupp, Metal-organic framework materials as catalysts, Chem. Soc. Rev. 38 (2009) 1450–1459, https://doi.org/10.1039/b807080f.
[14] Y. Zhang, S. Yuan, G. Day, X. Wang, X. Yang, H.C. Zhou, Luminescent sensors based on metal-organic frameworks, Coord. Chem. Rev. 354 (2018) 28–45, https://doi.org/10.1016/j.ccr.2017.06.007.
[15] H. Guo, N. Wu, R. Xue, H. Liu, L. Li, M. yue Wang, W. qin Yao, Q. Li, W. Yang, Multifunctional Ln-MOF luminescent probe displaying superior capabilities for highly selective sensing of Fe3+ and Al3+ ions and nitrotoluene, Colloids Surfaces A Physicochem. Eng. Asp. 585 (2020), https://doi.org/10.1016/j.colsurfa.2019.124094.
[16] X. Li, J. Tang, H. Liu, K. Gao, X. Meng, J. Wu, H. Hou, A highly sensitive and recyclable ln-MOF luminescent sensor for the efficient detection of Fe $^{3+}$ and Cr ^{VI} anions, Chem. Asian J. 14 (2019) 3721–3727, https://doi.org/10.1002/asia.201900936.
[17] H. Yu, M. Fan, Q. Liu, Z. Su, X. Li, Q. Pan, X. Hu, Two highly water-stable imidazole-based ln-MOFs for sensing Fe3+,Cr2O72-/CrO42- in a water environment, Inorg. Chem. 59 (2020), https://doi.org/10.1021/acs.inorgchem.9b03364, 2005–2010.
[18] Z. Sun, Y. Li, Y. Ma, L. Li, Dual-functional recyclable luminescent sensors based on 2D lanthanide-based metal-organic frameworks for highly sensitive detection of Fe3 + and 2,4-dinitrophenol, Dyes Pigments 146 (2017) 263–271, https://doi.org/10.1016/j.dyepig.2017.07.015.
[19] S. Pal, P.K. Bharadwaj, A luminescent terbium MOF containing hydroxyl groups exhibits selective sensing of nitroaromatic compounds and Fe(III) ions, Cryst. Growth Des. 16 (2016) 5852–5858, https://doi.org/10.1021/acs.cgd.6b00930.
[20] P.T. Lieu, M. Heiskala, P.A. Peterson, Y. Yang, The roles of iron in health and disease, Mol. Aspect. Med. 22 (2001) 1–87, https://doi.org/10.1016/S0098-2997(00)00006-6.
[21] P. Jia, Z. Wang, Y. Zhang, D. Zhang, W. Gao, Y. Su, Y. Li, C. Yang, Selective sensing of Fe3+ ions in aqueous solution by a biodegradable platform based lanthanide metal organic framework, Spectrochim. Acta Part A Mol. Biomol. Spectrosc. 230 (2020) 118084, https://doi.org/10.1016/j.saa.2020.118084.
[22] X. Zhang, Z. Zhan, X. Liang, C. Chen, X. Liu, Y. Jia, M. Hu, Lanthanide-MOFs constructed from mixed dicarboxylate ligands as selective multi-responsive luminescent sensors, Dalton Trans. 47 (2018) 3272–3282, https://doi.org/10.1039/c7dt02966g.
[23] S.-W. Lv, J.-M. Liu, C.-Y. Li, N. Zhao, Z.-H. Wang, S. Wang, A novel and universal metal-organic frameworks sensing platform for selective detection and efficient removal of heavy metal ions, Chem. Eng. J. 375 (2019) 122111, https://doi.org/10.1016/j.cej.2019.122111.
[24] C.D. Gutsche, The calixarenes, host guest complex, Chem./Macrocycles. (1985) 375–421, https://doi.org/10.1007/978-3-642-70108-5_9.
[25] B.M. Furphy, J.M.B. Harrowfield, M.I. Ogden, B.W. Skelton, A.H. White, F.R. Wilner, Lanthanide ion complexes of the calixarenes. Part 4. Double inclusion by p-t-butylcalix[4]arene (H4L). Crystal structures of [Eu2(HL)2(dmf)4]·7dmf (dmf = dimethylformamide) and H4L·dmso (dmso = dimethyl sulphoxide), J. Chem. Soc., Dalton Trans. (1989) 2217–2221, https://doi.org/10.1039/DT9890002217.
[26] A. Jäschke, M. Kischel, A. Mansel, B. Kersting, Hydroxyquinoline–Calix[4]arene conjugates as ligands for polynuclear lanthanide complexes: preparation, characterization, and properties of a dinuclear EuIIIComplex, Eur. J. Inorg. Chem. 2017 (2017) 894–901, https://doi.org/10.1002/ejic.201601326.
[27] R.F. Ziessel, L.J. Charbonnière, M. Cesario, T. Prangé, M. Guardigli, A. Roda, A. Van Dorsselaer, H. Nierengarten, p-tert-butylcalix[4]arene functionalised with bipyridyl carboxylates for lanthanide complexation: synthesis, photophysical properties, solution and solid state behavior, Supramol. Chem. 15 (2003) 277–289, https://doi.org/10.1080/1061027021000057224.

[28] Y.J. Liu, J.S. Huang, S.S.Y. Chui, C.H. Li, J.L. Zuo, N. Zhu, C.M. Che, A noncentrosymmetric 3D coordination polymer of metallocalix[4]arene, Inorg. Chem. 47 (2008) 11514–11518, https://doi.org/10.1021/ic8008859.
[29] S.P. Bew, A.D. Burrows, T. Düren, M.F. Mahon, P.Z. Moghadam, V.M. Sebestyen, S. Thurston, Calix[4]arene-based metal-organic frameworks: towards hierarchically porous materials, Chem. Commun. 48 (2012) 4824–4826, https://doi.org/10.1039/c2cc30988b.
[30] A. Ovsyannikov, S. Solovieva, I. Antipin, S. Ferlay, Coordination Polymers based on calixarene derivatives: structures and properties, Coord. Chem. Rev. 352 (2017) 151–186, https://doi.org/10.1016/j.ccr.2017.09.004.
[31] Y.-Y. Liu, C. Chen, J.-F. Ma, J. Yang, A series of complexes constructed by different calix[4]arene derivatives, CrystEngComm 14 (2012) 6201, https://doi.org/10.1039/c2ce25650a.
[32] R.S. Viana, C.A.F. Oliveira, J. Chojnacki, B.S. Barros, S. Alves, J. Kulesza, Structural and spectroscopic investigation of new luminescent hybrid materials based on calix[4]arene-tetracarboxylate and Ln3+ ions (Ln = Gd, Tb or Eu), J. Solid State Chem. 251 (2017) 26–32, https://doi.org/10.1016/j.jssc.2017.04.002.
[33] L.L. Liu, Z.G. Ren, L.W. Zhu, H.F. Wang, W.Y. Yan, J.P. Lang, Temperature-driven assembly of Ln(III) (Ln = Nd, Eu, Yb) coordination polymers of a flexible Azo Calix[4]arene polycarboxylate ligand, Cryst. Growth Des. 11 (2011) 3479–3488, https://doi.org/10.1021/cg200308k.
[34] Y. Bi, G. Xu, W. Liao, S. Du, R. Deng, B. Wang, Calixarene-supported hexadysprosium cluster showing single molecule magnet behavior, Sci. China Chem. 55 (2012) 967–972, https://doi.org/10.1007/s11426-012-4570-5.
[35] G. Karotsis, S. Kennedy, S.J. Teat, C.M. Beavers, D.A. Fowler, J.J. Morales, M. Evangelisti, S.J. Dalgarno, E.K. Brechin, Calix[4]arene clusters as enhanced magnetic coolers and molecular magnets, J. Am. Chem. Soc. 132 (2010) 12983–12990, https://doi.org/10.1021/ja104848m.
[36] G. Karotsis, S.J. Teat, W. Wernsdorfer, S. Piligkos, S.J. Dalgarno, E.K. Brechin, Calix[4]arene-based single-molecule magnets, Angew. Chem. Int. Ed. 48 (2009) 8285–8288, https://doi.org/10.1002/anie.200904094.
[37] Y. Bi, X.T. Wang, W. Liao, X. Wang, R. Deng, H. Zhang, S. Gao, Thiacalix[4]arene-supported planar Ln4 (Ln = TbIII, DyIII) clusters: toward luminescent and magnetic bifunctional materials, Inorg. Chem. 48 (2009) 11743–11747, https://doi.org/10.1021/ic9017807.
[38] C.R. Driscoll, B.L. Reid, M.J. McIldowie, S. Muzzioli, G.L. Nealon, B.W. Skelton, S. Stagni, D.H. Brown, M. Massi, M.I. Ogden, A "plug-and-play" approach to the preparation of transparent luminescent hybrid materials based on poly(methyl methacrylate), a calix[4]arene cross-linking agent, and terbium ions, Chem. Commun. 47 (2011) 3876–3878, https://doi.org/10.1039/c0cc05570k.
[39] X-Area WinXpose 2.0.22.0 (STOE, 2016), Darmstadt, Germany, (n.d.).
[40] G.M. Sheldrick, Shelxt - integrated space-group and crystal-structure determination, Acta Crystallogr. Sect. A Found. Crystallogr. 71 (2015) 3–8, https://doi.org/10.1107/S2053273314026370.
[41] G.M. Sheldrick, Crystal structure refinement with SHELXL, Acta Crystallogr. Sect. C Struct. Chem. 71 (2015) 3–8, https://doi.org/10.1107/S2053229614024218.
[42] O.V. Dolomanov, L.J. Bourhis, R.J. Gildea, J.A.K. Howard, H. Puschmann, OLEX2: a complete structure solution, refinement and analysis program, J. Appl. Crystallogr. 42 (2009) 339–341, https://doi.org/10.1107/S0021889808042726.
[43] C.F. Macrae, I.J. Bruno, J.A. Chisholm, P.R. Edgington, P. McCabe, E. Pidcock, L. Rodriguez-Monge, R. Taylor, J. van de Streek, P.A. Wood, *Mercury CSD 2.0* – new features for the visualization and investigation of crystal structures, J. Appl. Crystallogr. 41 (2008) 466–470, https://doi.org/10.1107/S0021889807067908.
[44] C.D. Gutsche, M. Iqbal, p - tert -Butylcalix[4]arene, Org. Synth. (2003) 234, https://doi.org/10.1002/0471264180.os068.29.
[45] F. Arnaud-Neu, G. Barrett, S. Cremin, M. Deasy, G. Ferguson, S.J. Harris, A.J. Lough, L. Guerra, M.A. McKervey, M.J. Schwing-Weill, P. Schwinte, Selective alkali-metal cation complexation by chemically modified calixarenes. Part 4. Effect of substituent variation on the Na +/K+ selectivity in the ester series and x-ray crystal structure of the trifluoroethyl ester, J. Chem. Soc. Perkin Trans. 2 (1992) 1119–1125, https://doi.org/10.1039/p29920001119.
[46] F. Arnaud-Neu, E. Marques, M.J. Schwing-Weill, E.M. Collins, M. Deasy, M.A. McKervey, E.M. Seward, G. Ferguson, B. Kaitner, A.J. Lough, B.L. Ruhl, S.J. Harris, Synthesis, X-ray crystal structures, and cation-binding properties of alkyl calixaryl esters and ketones, a new family of macrocyclic molecular receptors, J. Am. Chem. Soc. 111 (1989) 8681–8691, https://doi.org/10.1021/ja00205a018.
[47] K. Iwamoto, K. Araki, S. Shinkai, Syntheses of all possible conformational isomers of O-alkyl-p-t-butylcalix[4]arenes, Tetrahedron 47 (1991) 4325–4342, https://doi.org/10.1016/S0040-4020(01)87102-7.
[48] S. O'Malley, B. Schazmann, D. Diamond, K. Nolan, Preparation and sensor evaluation of a Pacman phthalocyanine, Tetrahedron Lett. 48 (2007) 9003–9007, https://doi.org/10.1016/j.tetlet.2007.10.089.
[49] H. Mighani, H. Tashakkorian, M. Mighani, Synthesis and characterization of soluble polyester based on calixarene dicarboxylic acid with tertiary butyl pendant groups, Chinese J. Polym. Sci. (English Ed. 32 (2014) 551–557, https://doi.org/10.1007/s10118-014-1430-0.
[50] K. Binnemans, Interpretation of europium(III) spectra, Coord. Chem. Rev. 295 (2015) 1–45, https://doi.org/10.1016/j.ccr.2015.02.015.
[51] A. Sengupta, S.V. Godbole, P.K. Mohapatra, M. Iqbal, J. Huskens, W. Verboom, Judd-Ofelt parameters of diglycolamide-functionalized calix[4]arene Eu 3+ complexes in room temperature ionic liquid for structural analysis: effects of solvents and ligand stereochemistry, J. Lumin. 148 (2014) 174–180, https://doi.org/10.1016/j.jlumin.2013.12.009.
[52] X.F. Qiao, H.Y. Zhang, B. Yan, Photoactive binary and ternary lanthanide (Eu3+, Tb 3+, Nd3+) hybrids with p-tert-butylcalix[4]arene derived Si-O linkages and polymers, Dalton Trans. 39 (2010) 8882–8892, https://doi.org/10.1039/c0dt00290a.
[53] H. Ebendorff-Heidepriem, D. Ehrt, Formation and UV absorption of cerium, europium and terbium ions in different valencies in glasses, Opt. Mater. 15 (2000) 7–25, https://doi.org/10.1016/S0925-3467(00)00018-5.
[54] H.L. Li, Z.L. Wang, S.J. Xu, J.H. Hao, Improved performance of spherical BaWO[sub 4]:Tb[sup 3+] phosphors for field-emission displays, J. Electrochem. Soc. 156 (2009) J112, https://doi.org/10.1149/1.3095503.
[55] Y. Shi, Y. Wen, M. Que, G. Zhu, Y. Wang, Structure, photoluminescent and cathodoluminescent properties of a rare-earth free red emitting β-Zn3B2O 6:Mn2+ phosphor, Dalton Trans. 43 (2014) 2418–2423, https://doi.org/10.1039/c3dt52405a.
[56] M. O'Toole, D. Diamond, Absorbance based light emitting diode optical sensors and sensing devices, Sensors 8 (2008) 2453–2479, https://doi.org/10.3390/s8042453.
[57] W. Wang, N. Gong, H. Yin, B. Zhang, P. Guo, B. Liu, Y.Y. Wang, Two stable terbium-organic frameworks based on predesigned functionalized ligands: selective sensing of Fe3+ ions and C2H2/CH4 separation, Inorg. Chem. 58 (2019) 10295–10303, https://doi.org/10.1021/acs.inorgchem.9b01465.
[58] H.H. Yu, J.Q. Chi, Z.M. Su, X. Li, J. Sun, C. Zhou, X.L. Hu, Q. Liu, A water-stable terbium metal-organic framework with functionalized ligands for the detection of Fe3+and Cr2O72-ions in water and picric acid in seawater, CrystEngComm 22 (2020) 3638–3643, https://doi.org/10.1039/d0ce00430h.